## Title

Proof-of-concept optimization of a copper-mediated 18 F-radiosynthesis of a novel MAGL PET tracer on a high-throughput microdroplet platform and its macroscale translation



## Journal

Lab on a Chip, 23(21)

## ISSN

1473-0197

## Authors

Lu, Yingqing
He, Yingfang
Schibli, Roger
et al.

## Publication Date

2023-10-24

## DOI

10.1039/d3lc00735a

Peer reviewed

HHS Public Access

Author manuscript

*Lab Chip*. Author manuscript; available in PMC 2024 October 24.

Published in final edited form as:

*Lab Chip*. ; 23(21): 4652–4663. doi:10.1039/d3lc00735a.

# Proof-of-concept optimization of a copper-mediated $^{18}$F-radiosynthesis of a novel MAGL PET tracer on a high-throughput microdroplet platform and its macroscale translation†

**Yingqing Lu**[a,b,c], **Yingfang He**[d], **Roger Schibli**[d], **Linjing Mu**[d], **R. Michael van Dam**[a,b,c]

[a]Crump Institute for Molecular Imaging, University of California Los Angeles (UCLA), Los Angeles, CA, USA.

[b]Department of Molecular & Medical Pharmacology, UCLA, Los Angeles, CA, USA

[c]Physics and Biology in Medicine Interdepartmental Graduate Program, UCLA, Los Angeles, CA, USA

[d]Center for Radiopharmaceutical Sciences, Institute of Pharmaceutical Sciences, Department of Chemistry and Applied Biosciences, ETH Zurich, Zurich, Switzerland

## Abstract

Copper-mediated radiofluorination has demonstrated remarkable potential in forming aromatic C–$^{18}$F bonds of radioligands for positron emission tomography (PET). Achieving optimal results often requires optimization efforts, requiring a substantial amount of radiolabeling precursor and time, severely limiting the experimental throughput. Recently, we successfully showcased the feasibility of performing and optimizing Cu-mediated radiosynthesis on a high-throughput microdroplet platform using the well-known and clinically used radioligand [$^{18}$F]FDOPA as an illustrative example. In our current work, we optimized the Cu-mediated synthesis of a novel monoacylglycerol lipase (MAGL) PET tracer ([$^{18}$F]YH149), showing the versatility of droplet-based techniques for early stage tracer development. Across 5 days, we conducted a total of 117 experiments, studying 36 distinct conditions, while utilizing <15 mg of total organoboron precursor. Compared to the original report in which the radiochemical yield (RCY) was 4.4 ± 0.5% ($n$ = 5), the optimized droplet condition provided a substantial improvement in RCY (52 ± 8%, $n$ = 4) and showed excellent radiochemical purity (100%) and molar activity (77–854 GBq μmol$^{-1}$), using a starting activity of 0.2–1.45 GBq. Furthermore, we showed for the first time a translation of the optimized microscale conditions to a vial-based method. With similar starting activity (0.2–1.44 GBq), the translated synthesis exhibited a comparable RCY of 50 ± 10% ($n$ = 4) while maintaining excellent radiochemical purity (100%) and acceptable molar activity (20–46

†Electronic supplementary information (ESI) available. See DOI: https://doi.org/10.1039/d3lc00735a

lyq@g.ucla.edu, mvandam@mednet.ucla.edu.

Author contributions

Y. L. fabricated the high-throughput microdroplet platforms. Y. H. synthesized the YH149 precursor and standard. Y. L., Y. H., R. S., L. M., and R. M. V. designed the experiments. Y. L. performed experiments and analyzed results and data. Y. H., R. S., L. M., and R. M. V. helped troubleshoot the purification issue of radiosynthesis. Y. L. and R. M. V. wrote the manuscript with input from Y. H., R. S., and L. M.

Conflicts of interest

Dr. van Dam is a co-founder of SOFIE, Inc. and DropletPharm, Inc.

GBq μmol$^{-1}$). The successful translation to vial-based reactions ensures wider applicability of the optimized synthesis by leveraging widely available commercial vial-based synthesis modules.

## 1. Introduction

Positron emission tomography (PET) is a vital nuclear imaging technique for studying *in vivo* biodistribution, diagnosing diseases, monitoring therapy response, and developing new drugs.[1] PET relies on positron–electron annihilation, generating gamma rays that are detected by PET scanners, and provides valuable insights into the binding and uptake behavior of radiolabeled compounds (*i.e.* radiotracers) to specific biomolecular targets.[2] Fluorine-18, with its favorable nuclear and physical properties such as high positron yield, low energy, short range, and suitable half-life, is widely used to label biomolecules for PET imaging.[3,4] Aromatic systems labeled with [$^{18}$F]fluorine, in particular, tend to offer good *in vivo* stability, making them ideal for PET tracer development.[5] Numerous approaches have been reported for 18F-labeling of aromatic compounds, though introducing [$^{18}$F]fluoride into neutral and electron-rich aromatic rings remains challenging.[4,6–8]

Currently, the Cu-mediated radiofluorination technique has emerged as a highly promising and primary method for introducing aromatic C–$^{18}$F bonds into both novel and established PET tracers.[9–19] This innovative approach successfully overcomes numerous challenges associated with conventional fluorination methods, such as the limited shelf life of precursors, difficulties in synthesizing labeling complexes, and the demanding synthesis conditions, making it a valuable and indispensable strategy for labeling aromatic systems with F-18.

Despite the wide scope of this method, achieving efficient manufacturing of specific tracers often requires extensive optimization efforts to consider the impact of various factors such as solvent system, phase transfer catalyst (PTC) or base type, precursor amount, copper mediator type, reaction temperature, labeling time *etc.*[20–23] However, current commercial radiosynthesizers designed for milliliter-scale reactions present limitations in terms of cost, hot cell operation, and limited synthesis capacity per day, largely hindering their contribution to intensive optimization endeavors. Additionally, to ensure reasonable reaction rates at the milliliter scale, significant amounts of precursors and other species are utilized, resulting in significant waste and challenges in downstream purification to remove excess reactants and by-products. In particular, in the case of Cu-mediated radiofluorination, the presence of protoarene impurities generated from competing protodeborylation reactions complicates high-performance liquid chromatography (HPLC) purification due to their similar chemical properties to the desired product, further exacerbating the challenges.[24]

Microfluidic devices have emerged as efficient, compact, and cost-effective platforms with great potential for diverse radiotracer production, leading to the development of various microfluidic tools in radiochemistry over the past 15 years.[25–29] These systems can be roughly divided into two categories: flow chemistry systems and microscale batch systems. Flow-based reactors have shown great effectiveness in synthesizing various radiopharmaceuticals,[30] but these setups rely on macroscale components for some synthesis steps (*e.g.*, radioisotope concentration and product purification), making them similar to

conventional radiosynthesizers in terms of size, shielding requirements, and operating volumes. Recent batch-based systems have been reported that can provide clinical amounts of numerous radiopharmaceuticals and offer improvements due to significantly lower volumes[31] and smaller system size as well as improved integration with upstream and downstream processes. A variety of batch approaches have been pursued, including microvial reactors,[32–34] channel-based devices with integrated isotope processing and purification,[35,36] and droplet-reaction systems.

Within our research group, we have focused on the latter because of its simplicity, speed and versatility and have developed several generations of semi- and fully automated droplet-based reaction chips, including EWOD,[37,38] passive transport chips,[39,40] and surface-tension trap chips.[41] These devices have demonstrated comparable yields to conventional approaches but with significantly shorter overall synthesis times and 100× reduction in precursor, and provide high molar activity, regardless of whether one is producing small or large (radioactivity amount) batches.[42–44] The enhanced speed is primarily attributed to an efficient chip surface heating and cooling system combined with low solution volumes during reaction and evaporation steps as well as microvolume purification (using analytical-scale HPLC) of <100 μL crude product, eliminating the need for semi-preparative HPLC. Notably, we have recently showcased the feasibility of Cu-mediated radiosynthesis in a microdroplet reactor using [$^{18}$F]FDOPA as an example, achieving substantial improvements in radiofluorination (crude RCY of 43 ± 2% ($n$ = 4) from fluorination conversion *via* TLC of 60 ± 4% and collection efficiency of 71 ± 2%) with only 150 nmol of precursor.[45]

In this work, we address two key remaining questions. Firstly, how useful is the droplet method for optimizing radiotracer synthesis through Cu-mediated radiofluorination at an early stage of radiochemical and preclinical development? Secondly, can the microscale optimized conditions be translated to macroscale radiosynthesis protocols to be compatible with currently available radiosynthesizer technologies, *i.e.*, existing vial-based modules? To address these questions, we conducted a study using a novel PET tracer ([$^{18}$F]YH149) targeting monoacylglycerol lipase (MAGL) as a proof of concept.[46] Designed and synthesized *via* a Cu-mediated route (Fig. 1A), [$^{18}$F]YH149 targets MAGL in the endocannabinoid system, a critical enzyme associated with inflammation, neurodegenerative disorders, and cancer. Evaluation of [$^{18}$F] YH149 in mice demonstrated excellent selectivity and specificity towards MAGL, along with significantly higher brain uptake in PET imaging compared to other reversible MAGL tracers,[46] indicating its promising potential for clinical translation. However, the low RCY (4.4 ± 0.5%, decay-corrected) obtained using a macroscale synthesis platform is suboptimal for further imaging trials, severely limiting multi-center collaborative studies and larger cohort investigations. The pressing need for synthesis improvement makes [$^{18}$F] YH149 an ideal candidate for a high-throughput microdroplet-based optimization study as well as an exploration of its translation to macroscale synthesis. In the present study, we systematically screened various $^{18}$F-labeling parameters to develop an improved radiosynthesis for [$^{18}$F] YH149 and subsequently explored the scaling of optimal conditions to a vial-based reaction.

# 2. Experimental

## 2.1 Materials

Tetrabutylammonium hydrogen carbonate ($TBAHCO_3$, 75 mM in ethanol) was purchased from ABX Advanced Biochemical Compounds (Radeberg, Germany). Tetrabutylammonium trifluoromethanesulfonate (TBAOTf, >99%), Kryptofix® 222 ($K_{222}$, >99%) and potassium oxalate ($K_2C_2O_4$, 99%) were purchased from Sigma-Aldrich (St. Louis, MO, USA). Tetraethylammonium trifluoromethanesulfonate (TEAOTf, >99%) was purchased from TCI America (Portland, OR, USA). Cesium carbonate ($Cs_2CO_3$, 99%), potassium carbonate ($K_2CO_3$, >99%), anhydrous pyridine (Py, 99.8%), anhydrous *N*,*N*-dimethylformamide (DMF, 99.8%), anhydrous *N*,*N*-dimethylacetamide (DMA, 99.8%), anhydrous dimethyl sulfoxide (DMSO, >99.9%), *n*-butanol (*n*BuOH, 99.9%), 1,3-dimethyl-2-imidazolidinone (DMI, >99.5%), anhydrous acetonitrile (MeCN, 99.8%), anhydrous ethyl alcohol (EtOH, >99.5%), phosphoric acid ($H_3PO_4$, >85 wt% in $H_2O$) and tetrakis(pyridine)copper(II) triflate ($Cu(OTf)_2(Py)_4$, 95%) were purchased from Sigma-Aldrich (St. Louis, MO, USA). *N*-Methyl-2-pyrrolidone (NMP, >99%) was purchased from TCI America (Portland, OR, USA). The precursor and reference standard were prepared as previously reported.[46] Deionized (DI) water was obtained from a Milli-Q water purification system (EMD Millipore Corporation, Berlin, Germany). C18 plus light cartridges (130 mg sorbent, WAT023501) were purchased from Waters Corporation (Milford, MA, USA). Reagent and collection vials were purchased from Eppendorf (Hamburg, Germany). Reaction vials (4 mL) for macroscale reactions were purchased from Chemglass Life Sciences (CG-4904-06, Vineland, NJ, USA). Silicone oil (CAS 63148-62-9) used in the vial heating block was purchased from Fisher Chemical (Pittsburgh, PA, USA). 50 mL polypropylene centrifuge tubes were purchased from Corning Inc. (430 304, Corning, NY, USA). [$^{18}$F]Fluoride in [$^{18}$O]$H_2O$ was obtained from the UCLA Crump Cyclotron and Radiochemistry Center. The activity was used directly as provided by cyclotron without further purification for both droplet-based microscale and vial-based macroscale radiosynthesis.

## 2.2 Droplet-based radiosynthesis of [$^{18}$F]YH149

Droplet-based reactions were performed on Teflon-coated silicon chips patterned with 2 × 2 or 4 × 4 arrays of multiple hydrophilic reaction sites (Fig. 1B), operated on a temperature-controlled heating platform, as previously described.[47]

The general synthesis process (Fig. 1C) was as follows: 10 μL of an [$^{18}$F]fluoride stock solution (containing 23–170 MBq of activity mixed with a desired amount of PTC and base) was delivered *via* micropipette onto a reaction site of the chip and dried at 105 °C for 1 min. Next, 10 μL of a precursor/$Cu(OTf)_2(py)_4$ stock solution was added *via* micropipette and heated to perform the fluorination. After synthesis, the crude product was extracted from the reaction site by adding a collection solution (20 μL) and transferring *via* micropipette to a 0.5 mL Eppendorf tube for further analysis. The collection step was repeated a total of 4× to minimize activity residue on the chip. Studies were performed to optimize the reaction solvent type, PTC/base type and amount, reaction temperature, reaction time, and precursor amount.

Several stock solutions were prepared just prior to each batch of experiments. Stock solutions of PTC and base were prepared in DI water at concentrations such that a 5 μL aliquot contained the desired amount of PTC and base for a single droplet reaction. The amounts were optimized as part of this study. [$^{18}$F]Fluoride stock solution was prepared by mixing [$^{18}$F] fluoride/[$^{18}$O]$H_2O$ with the desired PTC/base stock solution in 1 : 1 (v/v) ratio, such that each 10 μL portion contained 23–170 MBq of activity along with the desired amount of PTC and base for a single reaction. Stock solutions of precursor (37 mM) and $Cu(OTf)_2(Py)_4$ (136 mM) were separately prepared in the desired reaction solvent mixture. These components were mixed in 1 : 1 (v/v) ratio just prior to synthesis such that each 10 μL portion of the mixed solution contained 0.185 μmol (0.1 mg) of precursor and 0.68 μmol of $Cu(OTf)_2(Py)_4$. In studies of precursor amount, a similar procedure was followed except the concentration of the precursor stock solution was varied. Collection solution was prepared by mixing MeCN and DI water (6 : 4, v/v).

In some cases (for comparison of performance of droplet and vial-based reactions), droplet reactions were prepared at higher activity scale. In these cases, 20 μL of [$^{18}$F]fluoride (0.2–1.45 GBq with the optimal PTC/base amount) was dried on the chip for a slightly longer time (~1.5 min), followed by the optimal fluorination process. The crude product was collected as described above, but using HPLC mobile phase (composition described below), followed by analytical-scale HPLC purification.

### 2.3 Macroscale production of [$^{18}$F]YH149

Macroscale synthesis was performed in a 4 mL GC vial. Heat was provided by placing the vial into a preheated aluminum vial block (Ohaus 30 400 185, Hogentogler & Co. Inc., Columbia, MD, USA) filled with 2 mL silicone oil. The vial block was heated on a hot plate (PC-420D, Corning Inc., Corning, NY, USA) equipped with a temperature probe (6795PR, Corning Inc., Corning, NY, USA) inserted into the heating block.

The droplet-based synthesis was implemented as a vial-based reaction by scaling up reagent amounts of the optimal conditions by 10× and performing reactions in 300 μL of reaction solvent mixture, but otherwise maintaining the same conditions as the droplet reaction. 20 μL of aqueous [$^{18}$F] fluoride (0.2–1.44 GBq), mixed with 10× the optimized amounts of PTC and base, was added to the reactor and dried at 105 °C until all liquid evaporated. Azeotropic drying was performed three times, each time by adding MeCN (30 μL) and drying at the same temperature. Stock solutions of precursor and $Cu(OTf)_2(Py)_4$ were each prepared in the optimized solvent system and were mixed in a 1 : 1 (v/v) ratio right before synthesis. 300 μL of the resulting mixture (containing 10× the amounts of precursor and $Cu(OTf)_2(Py)_4$ as the optimized droplet reaction) was added into the reaction vial and heated to the fluorination temperature *via* the heating block. The reaction was sampled at different time points to monitor its fluorination progress. At each time point, the reaction vial was moved from the heat block and cooled in a water bath (~20 °C) for ~1 min, and a 0.5 μL sample was taken from the reaction mixture and diluted with 20 μL of collection solution for TLC analysis. After taking the sample, the reaction vial was put back into the heat block until the next time point. After the 0.5 μL sample was taken from the final reaction mixture, the reaction mixture was quenched with 1 mL of DI water, transferred to a 50 mL centrifuge

tube and further diluted with 20 mL of DI water. Prior to HPLC purification, the solvent was exchanged by loading the diluted crude product on a light C18 cartridge (preconditioned with 5 mL of EtOH and then 20 mL of DI water), washing with 6 mL of DI water, and eluting with 0.5 mL of MeCN. The eluate was further concentrated to <0.1 mL by heating at 60 °C in a v-vial, enabling the crude product to be purified *via* analytical-scale HPLC.

### 2.4 Analytical equipment and methods

Radioactivity measurements were conducted using a calibrated dose calibrator (CRC-25R, Capintec, Florham Park, NJ, USA). Fluorination conversion was assessed *via* multi-lane radio-thin layer chromatography (radio-TLC) methods.[48] Briefly, samples (0.5 μL) were spotted on TLC plates (6 cm × 5 cm pieces cut from 20 cm × 5 cm sheets, silica gel 60 $F_{254}$, Merck KGaA, Darmstadt, Germany). Plates were developed for a 4 cm distance using a mobile phase of MeCN and DI water (7 : 3, v/v), dried, and then covered with a glass microscope slide (75 mm × 50 mm × 1 mm, Fisher Scientific, Hampton, NH, USA) and read out by Cerenkov luminescence imaging (CLI) with 5 min exposure time. Fluorination conversion of each sample (lane) was determined *via* ROI analysis as previously described.[48] Collection efficiency was obtained by dividing the activity of product mixture collected from the droplet or vial reactor by the starting activity (corrected for decay). Crude RCY was computed as fluorination conversion multiplied by the collection efficiency. The isolated RCY was determined by performing radio-HPLC purification on an analytical column (ZORBAX RP Eclipse Plus C18, 100 × 4.6 mm, 3.5 μm, Agilent Technologies, Santa Clara, CA, USA) using an isocratic mobile phase of DI water and MeCN (74 : 26, v/v) with 0.1% $H_3PO_4$ (v/v) at a flow rate of 1.2 mL $min^{-1}$. The radio-HPLC system comprised a Smartline HPLC system (Knauer, Berlin, Germany) equipped with a degasser (model 5050), pump (model 1000), UV detector (254 nm; Eckert & Ziegler, Berlin, Germany), gamma-radiation detector (BFC-4100, Bioscan, Inc., Poway, CA, USA), and counter (BFC-1000; Bioscan, Inc., Poway, CA, USA). The purified [$^{18}$F]YH149 was analyzed on the same radio-HPLC system to confirm radiochemical purity (RCP) using a mobile phase of DI water and MeCN (70 : 30, v/v) with 0.1% $H_3PO_4$ (v/v) at a flow rate of 1.2 mL $min^{-1}$. Co-injection of the purified [$^{18}$F]YH149 and reference standard was performed to confirm product identity. The same analytical-scale radio-HPLC system was employed to determine the molar activity of the purified [$^{18}$F]YH149, utilizing a linear calibration curve of YH149 reference standard. The comprehensive measurement details can be found in the ESI,† section 3.

## 3. Results and discussion

### 3.1 Optimization of [$^{18}$F]YH149 radiosynthesis using droplet reactions

**3.1.1 Initial conditions.—**As a starting point for droplet-based synthesis of [$^{18}$F]YH149, we tried two sets of conditions. First (condition 1), we scaled down the macroscale synthesis method described by He *et al.*[46] from 300 μL to 10 μL with 10× reduced reagents while preserving ingredient ratios except for $Cu(OTf)_2(Py)_4$ (we used 30× less instead of 10× less due to solubility issues). Second (condition 2), we used our previously reported droplet-based conditions for the Cu-mediated synthesis of [$^{18}$F]FDOPA[45] but used the [$^{18}$F]YH149 precursor. The detailed conditions and performance

of the reactions can be found in Table S1.† Surprisingly, our attempts to produce [$^{18}$F]YH149 by condition 1 yielded no product ($n$ = 2) (Fig. S1†). To our delight, we successfully obtained [$^{18}$F]YH149 by using condition 2, with moderate fluorination conversion of 44 ± 1% ($n$ = 2), good collection efficiency of 81 ± 2% ($n$ = 2) and crude RCY of 36 ± 2% ($n$ = 2). Despite this initial attempt already exceeding the performance of the vial-based reaction conditions,[46] we proceeded with further optimization starting with condition 2.

Noticing that the main differences between conditions 1 and 2 were reaction solvent composition and the type and amount of PTC/base, we focused initial optimization studies on these parameters and systematically explored various parameters in the following order: (1) solvent type, (2) type of PTC and base, (3) reaction temperature, (4) fluorination time, and (5) precursor amount. At each stage of optimization, we selected the best-performing condition, which was then fixed for subsequent experiments.

**3.1.2 Influence of reaction solvent.—**Various solvent systems were investigated for the preparation of [$^{18}$F]YH149 (Fig. 2A). Details of measurements and calculations are tabulated in Table S2,† and the CLI readout of the multi-lane TLC is shown in Fig. S2.† All reactions were conducted with TEAOTf (0.3 μmol)/$Cs_2CO_3$ (0.01 μmol) as PTC/base, $Cu(py)_4(OTf)_2$ (0.68 μmol) as copper reagent and 0.1 mg (0.18 μmol) of precursor in 10 μL solvent at 110 °C for 5 min. Among the different solvent systems tested, the mixed solvent DMA/*n*BuOH/pyridine (64 : 32 : 4, v/v) provided the best performance, with a fluorination conversion of 49 ± 2% ($n$ = 3), collection efficiency of 75 ± 1% ($n$ = 3) and crude RCY of 35 ± 0% ($n$ = 3). Notably, the absence of pyridine (*i.e.*, using only DMA/*n*BuOH (2 : 1, v/v)) resulted in a fluorination conversion of 0% ($n$ = 2), suggesting that pyridine is a critical additive for the formation of the radiofluorinated product. Pyridine likely serves as a stabilizer to maintain the functionality of the copper catalyst solution under ambient conditions, and its necessity was also mentioned by Mossine *et al.* in previous reports.[16,24]

**3.1.3 Influence of PTC/base.—**The next investigation involved different types of PTCs and bases (Fig. 2B). The detailed measurements and calculations can be found in Table S3† and multi-lane TLC data are shown in Fig. S3.† In the absence of base ($Cs_2CO_3$), the reaction with TEAOTf exhibited the highest fluorination conversion among the three PTCs tested, achieving 36 ± 1% ($n$ = 3) along with a good collection efficiency of 70 ± 1% ($n$ = 3) and resulting crude RCY of 25 ± 1% ($n$ = 3). The use of TBAOTf or $TBAHCO_3$ as the PTC exhibited significantly lower fluorination conversion, resulting in substantially lower crude RCY (19 ± 6%, $n$ = 3 for TBAOTf and 14 ± 1%, $n$ = 3 for $TBAHCO_3$). The addition of the base $Cs_2CO_3$ further improved the fluorination conversion (44 ± 3%, $n$ = 3 for TEAOTf/$Cs_2CO_3$ and 36 ± 2%, $n$ = 3 for TBAOTf/$Cs_2CO_3$), resulting in higher crude RCYs of 31 ± 3% ($n$ = 3) for TEAOTf/$Cs_2CO_3$ and 26 ± 4% ($n$ = 3) for TBAOTf/$Cs_2CO_3$, respectively. Hence, TEAOTf was identified as the optimal PTC for preparing [$^{18}$F]YH149, and the addition of base ($Cs_2CO_3$) was also important for a good manufacture.

**3.1.4 Effect of temperature and base type.—**We conducted additional investigation into the fluorination temperatures (Fig. 3A and B). As a mild and common base source in aprotic solvents, we also opted to explore $K_2CO_3$ as an alternative to $Cs_2CO_3$ in this

temperature study. A comprehensive listing of measurements and calculations and multi-lane radio-TLC images can be found in Tables S4 and S5 and Fig. S4 and S5,† respectively. In the presence of $Cs_2CO_3$, the fluorination conversion exhibited a significant increase with temperature, reaching a maximum of 78 ± 1% ($n$ = 3) at 140 °C. However, it was observed that higher temperatures led to increased volatile losses, resulting in a decline in the collection efficiency. The overall crude RCY demonstrated a sharp increase with temperature, rising from 21 ± 1% ($n$ = 3) at 100 °C to 40 ± 2% ($n$ = 3) at 120 °C, and then tended to stabilize beyond 120 °C. The maximum crude RCY of 43 ± 1% ($n$ = 3) was achieved at 140 °C, accompanied by a fluorination conversion of 78 ± 1% ($n$ = 3) and a collection efficiency of 55 ± 1% ($n$ = 3). When $K_2CO_3$ was used as the base (tested over a slightly higher temperature range), the fluorination conversion showed a small rise with increasing temperature; however, the collection efficiency exhibited a gradual decrease, with a net overall result of gradually decreasing crude RCY. At 160 °C, a more significant drop in reaction performance was observed. Nearly the best crude RCY occurred at 140 °C, where the fluorination efficiency was 67 ± 1% ($n$ = 3), collection efficiency was 57 ± 3% ($n$ = 3) and crude RCY was 38 ± 2% ($n$ = 3). Considering the higher volatile losses observed with $Cs_2CO_3$ at 140 °C (collection efficiency: 55 ± 1%, $n$ = 3 *vs.* 57 ± 3%, $n$ = 3 for $K_2CO_3$) and its more basic property in aprotic solvents,[49] we adopted $K_2CO_3$, the milder base, as the base for further experiments.

**3.1.5 Effect of reaction time.—**Next, we investigated the impact of reaction time (Fig. 3C). Detailed measurements and calculations and radio-TLC analysis can be found in Table S6 and Fig. S6.† We observed that radiofluorination proceeded rapidly within the first 2 min, followed by gradual growth, but collection efficiency showed an inverse trend, with increasing loss of volatile activity during longer reaction times. The resulting crude RCY exhibited a peak at 3 min, with a value of 42 ± 2% ($n$ = 3).

**3.1.6 Effect of base amount.—**Based on the optimal reaction time, a study of different amounts of base was conducted (Fig. 3D). Details of measurements and calculations and radio-TLC images can be found in Table S7 and Fig. S7.† We observed that increased amount of the base led to a gradual decrease in fluorination conversion, while the collection efficiency did not exhibit significant changes, resulting in a gradual decline in crude RCY. Based on these results, minimal use of base (10 nmol) was selected for the next optimization stage.

**3.1.7 Influence of precursor amount.—**We further explored the influence of precursor amount (Fig. 3E). Detailed measurements and calculations and radio-TLC images can be found in Table S8† and Fig. 4, respectively. Interestingly, the amount of precursor had only a slight impact on the various measures of performance of the reaction. Using 0.15 mg of precursor gave the highest overall crude RCY (42 ± 4%, $n$ = 3).

**3.1.8 Additional tests.—**Inspired by a separate study, in which we saw significantly improved production of [$^{18}$F] FBnTP achieved by using DMI as a solvent instead of DMA,[50] we conducted additional tests for the synthesis of [$^{18}$F] YH149. When replacing DMA with DMI under the fixed conditions derived from previous optimization stages (Table

S8 and Fig. S8†), the synthesis showed higher fluorination conversion (71 ± 5%, $n$ = 3 for DMI *vs.* 62 ± 2%, $n$ = 3 for DMA, $n$ = 3); however, collection efficiency was lower (57 ± 1%, $n$ = 3 for DMI *vs.* 68 ± 4%, $n$ = 3 for DMA), resulting in an overall lower crude RCY of 40 ± 4% ($n$ = 3) compared to 42 ± 4% for DMA. Therefore, we retained DMA/*n*BuOH/Py as the optimal solvent combination. Additionally, given the superior performance of $Cs_2CO_3$ compared to $K_2CO_3$ in the same [$^{18}$F] FBnTP study,[50] we were curious to compare these bases again for the preparation of [$^{18}$F]YH149 (Table S8 and Fig. S8†). To our surprise, the use of $Cs_2CO_3$ exhibited a significant increase in both fluorination conversion (80 ± 2%, $n$ = 4) compared to $K_2CO_3$ (62 ± 2%, $n$ = 3) and collection efficiency (71 ± 3%, $n$ = 4) compared to $K_2CO_3$ (68 ± 4%, $n$ = 3). Consequently, this configuration yielded the highest crude RCY of 56 ± 3% ($n$ = 4) compared to $K_2CO_3$ (42 ± 4%, $n$ = 3). As a result, we selected $Cs_2CO_3$ as the optimal base type.

**3.1.9 Overall synthesis including purification.—**Overall, as summarized in Table 1, 36 distinct conditions (totaling 117 experiments when replicates are included) were explored over a span of 5 days, consuming a total of <15 mg of precursor. In order to account for potential interfering factors (*e.g.* variations in [$^{18}$F]fluoride quality from day to day, batch-to-batch inconsistencies in stock solution preparation, *etc.*), each optimization experiment included conditions that repeated data points from the previous day as a control. We found such replicated measurements to be remarkably consistent, suggesting little impact of fluoride quality and batches of reagents. Each experimental reaction was performed with starting activity ranging from 22 to 170 MBq. The optimal process involved drying [$^{18}$F]fluoride with TEAOTf (0.3 μmol) and $Cs_2CO_3$ (0.01 μmol) at 105 °C for 1 min. No azeotropic drying steps were necessary. Subsequently, the fluorination reaction was performed at 140 °C for 3 min using 0.15 mg (0.28 μmol) of precursor and 0.68 μmol of $Cu(OTf)_2(Py)_4$ in a 10 μL solvent mixture of DMA/BuOH/pyridine (64 : 32 : 4, v/v). This optimized method achieved fluorination conversion (80 ± 2%, $n$ = 3) and collection efficiency (71 ± 3%, $n$ = 3) at the end of the reaction, resulting in a crude RCY of 56 ± 3% ($n$ = 3). The optimized synthesis was then scaled to higher activities (0.2 to 1.45 GBq) and combined with purification. Taking advantage of the microscale radiosynthesis, the collected crude product volume (~80 μL) and reagent mass were sufficiently low that purification was possible using an analytical radio-HPLC system under isocratic conditions. Purified product could be collected in ~20 min. The radio-HPLC chromatogram of the crude [$^{18}$F] YH149 injection showed excellent separation resolution (Fig. 5A). The isolated RCY (52 ± 8%, $n$ = 4) closely matched the calculated crude RCY (56 ± 3%, $n$ = 3; based on radio-TLC measurement), suggesting minimal residual losses during the HPLC injection and purification process. The radiochemical purity of the purified [$^{18}$F]YH149 was 100%, determined by radio-HPLC (using the analytical mobile phase). Fig. 5B shows an HPLC chromatogram of a blank injection of the purification mobile phase (20 μL), and Fig. 5C shows a chromatogram of the injected purified product (20 μL). Co-injection of the purified [$^{18}$F]YH149 and the reference standard confirmed the product identity (Fig. 5D). Note that the analytical mobile phase had higher organic content (30% *vs.* 26% MeCN); thus the retention time is lower (8.5 min *vs.* 18.6 min). The molar activity at the end of synthesis was determined to be 77–854 GBq μmol$^{-1}$. The overall synthesis time was 26 min, comprising 6 min for radiolabeling and 20 min for purification.

The performance is summarized in Table 2 and compared to the results of the originally reported macroscale synthesis,[46] highlighting notable improvements in synthesis time and RCY. One reason for the improved RCY at the microscale could be the increased precursor concentration (28 mM *vs.* 12.3–18.3 mM). Despite this increased concentration, we achieved a 13–20× reduction in precursor consumption by using a significantly smaller reaction volume (10 *vs.* 300 μL). The concentration of the copper reagent was similar (68 mM for the microscale reaction *vs.* 68.7 mM in He *et al.*[46]), but the total amount was ~30× lower due to the reduced reaction volume. The reduced reagent usage significantly reduced the formation of side products, resulting in simplified purification. The elevated temperature (140 °C in this work *vs.* 110 °C in ref. 46) likely also played a role in improving performance. Only two major radio-peaks, corresponding to unreacted [$^{18}$F]fluoride and [$^{18}$F]YH149, were seen in the HPLC chromatogram from the crude droplet reaction (Fig. 5A). Furthermore, the UV chromatogram showed only a few impurities in very low quantities, well separated from the product peak. Notably, purification could be streamlined on an analytical-scale HPLC with an isocratic mobile phase, while the conventional radiosynthesis method required a gradient protocol, leading to the need for a more complex HPLC setup. Overall, the droplet synthesis exhibited a ~12-fold increase in RCY (52 ± 8%, $n$ = 4) compared to the previous macroscale approach (4.4 ± 0.5%, $n$ = 4). Moreover, despite commencing with significantly lower initial activity compared to the conventional macroscale approach (0.2–1.45 GBq *vs.* 50–60 GBq), the droplet method achieved high molar activity ranging from 77 to 854 GBq μmol$^{-1}$ at the end of synthesis. Furthermore, despite using ~41× lower starting activity, the droplet reaction could still produce enough product amount for preclinical and clinical studies. This high-performing microscale synthesis paves the way for efficient production of small tracer batches through Cu-mediated radiofluorination, delivering the high molar activity needed for preclinical imaging scenarios. Sufficient product amount of [$^{18}$F]YH149 (80–623 MBq) was also obtained for multiple preclinical imaging studies or a single patient scan for a clinical study. Finally, the total preparation time using the droplet method was merely one-third of that required by the conventional method, resulting in significant time savings.

### 3.2 Translation of microscale conditions to vial-based reaction

Although we have previously shown the possibility of performing relatively large scale (multiple patient doses) in individual droplet reactions,[51,52] we understand that droplet reactor systems are not currently widely available, preventing others from taking advantage of the improved synthesis process. Therefore, we decided to explore the potential of directly scaling the optimized droplet conditions to a vial-based (macroscale) reaction.

To continue to leverage the benefits of isolating the crude product *via* an analytical radio-HPLC system (*i.e.* excellent separation capabilities and shorter purification time), we minimized the reagent use in the macroscale reaction by employing only a 10× scale-up of all reagents (*i.e.* 3 μmol of TEAOTf, 0.1 μmol of $Cs_2CO_3$, 2.8 μmol of precursor, and 6.8 μmol of $Cu(Py)_4(OTf)_2$) while increasing the reaction volume 30× from a 10 μL droplet to a 300 μL vial-based reaction. In order to ensure a sufficiently small volume for injection into analytical HPLC, we needed to add a solvent-exchange step after the fluorination step (from

reaction solvent to MeCN) and then an evaporative concentration step to reduce the volume. The overall process flow of the macroscale reactor synthesis is depicted in Fig. S9.†

The performance and duration of each step in the macroscale synthesis are summarized in Table S9.† To enable comparisons to the droplet reaction, the synthesis used a comparable activity level (0.2–1.44 GBq) and the same volume of aqueous [$^{18}$F]fluoride. The aliquot was mixed with 5 μL of PTC/base (10× more concentrated), added to the vial, and heated at 105 °C for evaporation. It took ~5 min to evaporate most of the initial 25 μL solution. Since a tiny amount of liquid remained on the bottom of the vial even after the extra heating time, azeotropic drying was conducted with 30 μL of MeCN (repeated 3×), taking an additional ~6 min. It took ~1 min to cool the vial to room temperature in a water bath after each evaporation. Due to the macroscale reaction solution being more dilute than the microscale reaction (3× less due to 30× volume increase but only 10× reagent increase), we anticipated a potential decrease in reaction rate as well as slower mixing and heating in the macroscale reactor, and a potential need to increase the reaction time. To monitor the progress of the macroscale reaction, 0.5 μL samples were taken at different time points (3, 6, and 10 min) to measure the fluorination conversion (Fig. S10†). The reaction exhibited a high fluorination conversion of 69 ± 1% ($n$ = 4) within the first 3 min, which increased to 76 ± 1% ($n$ = 4) at 6 min. Beyond 10 min, the fluorination conversion exhibited only a slight increase, reaching 77 ± 2% ($n$ = 4), prompting the reaction to be stopped after 10 min.

Following the 10 min reaction, 81 ± 5% ($n$ = 4) of the starting activity (corrected for decay) was successfully extracted into a collection vial. 17 ± 4% ($n$ = 4) of the starting activity remained in the reactor and the reactor cap, despite attempts to extract it using additional water (1 mL) or MeCN (1 mL). The collected activity was further diluted with DI water and loaded onto a light C18 cartridge, followed by washing with an additional 6 mL of DI water to remove unreacted [$^{18}$F]fluoride. Around 52 ± 10% ($n$ = 4) of the starting activity was trapped on the cartridge, and the waste activity resulting from the trapping and washing procedure was 27 ± 11% ($n$ = 4) of the starting activity. Using 0.5 mL of MeCN, most of the activity was eluted off the cartridge, *i.e.*, 51 ± 10% of the starting activity was recovered with minimal residual activity on the cartridge (1 ± 0%, $n$ = 4). The eluted activity was then concentrated to less than 0.1 mL by heating at 60 °C. The concentrated reaction mixture was purified using analytical-scale radio-HPLC in ~13 min, resulting in an isolated RCY of 50 ± 10% ($n$ = 4, Table 2), suggesting negligible losses during the purification step. An example HPLC chromatogram during the purification process is shown in Fig. S12.† According to radio-HPLC measurements, the purified [$^{18}$F]YH149 exhibited a radiochemical purity of 100% (Fig. S13†), and the molar activity at the end of synthesis was determined to be 20–46 GBq μmol$^{-1}$. The co-injection of purified [$^{18}$F]YH149 and the reference standard confirms the chemical identity from this macroscale synthesis (Fig. S14†). The overall preparation time was ~58 min, including 15 min for [$^{18}$F]fluoride drying, 15 min for radiofluorination, 15 min for crude product concentration, and 13 min for purification.

To ensure a fair and direct comparison between the optimized droplet method and the translated vial-based method, both were conducted on the same day, employing identical amounts of [$^{18}$F]fluoride loaded manually to eliminate any possible interference (like [$^{18}$F]fluoride losses within fluidic pathways from a QMA process), and using the aliquots

of the same batch of radioisotope, precursor and copper reagent (the stock solutions for the precursor and $Cu(Py)_4(OTf)_2$ had to be diluted to the appropriate concentration for the macroscale reaction). The translated macroscale synthesis yielded a high RCY of 50 ± 10% ($n$ = 4), nearly identical to that achieved by the droplet method (52 ± 8%, $n$ = 4). One notable difference is that the molar activity obtained from the translated macroscale synthesis was 4–18× lower than that achieved with the droplet method (20–46 GBq μmol$^{-1}$ *vs.* 77–854 GBq μmol$^{-1}$), despite starting with the same initial activity. This discrepancy suggests the presence of non-radioactive fluoride contamination, likely from the vial materials and/or reagents and solvents, and can likely be overcome by starting with a higher activity scale.[44] Another difference is that the translated macroscale synthesis needed double the preparation time due to additional required processes, such as azeotropic drying and crude product concentration. Interestingly, the purification time was shortened to 13 min (Fig. S9†) (compared to 20 min for the droplet method in Fig. 5A) since the product peak emerged earlier upon injection of the crude product when dissolved in 100% MeCN, *versus* when it is dissolved in the collection solution as was the case for the droplet reactions. This suggests that the purification time for the droplet reaction could in fact be further reduced by an optimized collection solution or HPLC mobile phase, shrinking the overall preparation time.

If we compare our droplet-to-vial translated protocol with the previously reported macroscale conditions of He *et al.*,[46] interesting findings emerge. Although both approaches used the same reaction volume (300 μL), this approach required lower concentrations of precursor (9.3 mM *vs.* 12.3 mM) and $Cu(Py)_4(OTf)_2$ (22.7 mM *vs.* 68.7 mM), yet it delivered an impressive 11-fold increase in RCY. We should point out that the amount of PTC (3 μmol) and base (0.1 μmol) used in the translated vial-based method was slightly lower than the quantities of PTC/base typically utilized to achieve efficient [$^{18}$F]fluoride elution from QMA cartridges for Cu-mediated synthesis in the same co-solvent system, *e.g.* as reported by Zlatopolskiy *et al.* (using ~14 μmol of $TEAHCO_3$)[53] and Hoffmann *et al.* (using 4 μmol of TEAOTf).[23] Since a lower amount of PTC and base can adversely impact the efficiency of eluting [$^{18}$F]fluoride from a QMA cartridge, we performed an additional study of different elution conditions (in MeOH : water solvent mixture) and found that >99% elution efficiency could be achieved with an increased amount (12 μmol) of TEAOTf and no change in the amount of $Cs_2CO_3$ (0.1 μmol). We tested in droplet reactions the effect of the larger TEAOTf amount and found comparable performance. Thus, these reports suggest that the current translated vial-based recipe would be compatible with conventional synthesizers using QMA-cartridge processing without significant need for further adjustments other than the drying process for the [$^{18}$F]fluoride/PTC/base complex.

Additionally, these results represent a successful demonstration of using droplet-based methods for optimization (which can be performed with high throughput and very low reagent consumption), and then adapting those optimal reaction conditions to a macroscale process with minimal modification. This shows the current utility of using high-throughput droplet-based reaction optimization, even when the vast majority of installed radiotracer production systems currently rely on vial-based reactions. The 300 μL reaction volume (selected to match previously reported vial-based conditions), though at the low end of the

volume capability of modern radiosynthesizers (300–500 μL),[15,20,46,54,55] suggests that this protocol could be automated using widely available radiosynthesis systems easily.

Building upon the successful macroscale translation experience presented in this study, further investigations could be conducted to explore the versatility of micro-to-macroscale translation for other tracers synthesized through Cu-mediated routes, such as [$^{18}$F]FDOPA and [$^{18}$F]FBnTP, as well as different radiolabeling mechanisms like [$^{18}$F]FET, [$^{18}$F]flumazenil, and [$^{18}$F]PBR06. This would contribute to expanding our understanding of the translation process and its applicability to various radiotracers. Moreover, the scaling up of radiosynthesis using the droplet-based optimized condition on a conventional automated system to achieve multiple clinical doses would be of great interest to the radiochemistry community. Currently, the field has extremely limited approaches for increasing optimization throughput that are applicable to macroscale radiosynthesis, and thus this droplet-to-vial-based approach demonstrated here could fill a much-needed gap to streamline the development and production of novel tracers from initial synthesis through clinical studies.

## 4. Conclusions

In this work, we used a novel droplet-based high-throughput technique to perform a rapid optimization of Cu-mediated radiosynthesis for the recently reported monoacylglycerol lipase PET tracer [$^{18}$F]YH149. A total of 117 experiments were performed across 5 days to explore 36 distinct conditions while consuming <15 mg total amount of precursor. The optimized synthesis exhibited a high radiochemical yield of up to 52 ± 8% ($n$ = 4) in a 26 min process, with excellent radiochemical purity (100%) and high molar activity (77–854 GBq μmol$^{-1}$), providing significant improvement upon the originally reported conditions based on a 300 μL vial-based reaction (with RCY of 4.4 ± 0.5%, $n$ = 5). In conjunction with prior results of droplet-based optimization for [$^{18}$F]FDOPA[45] and [$^{18}$F]FBnTP,[50] the results suggest that the droplet-based technique is well-suited to Cu-mediated radiosyntheses of $^{18}$F-labeled tracers.

In addition, we demonstrated for the first time the successful translation of the optimized droplet conditions to a vial-based (macroscale) reaction. By simply scaling reagent amounts by 10× and extending reaction time to an optimal value based on a single time-course study, we observed that a 300 μL vial-based reaction had similar RCY to the microscale method, *i.e.*, 50 ± 10% ($n$ = 4), excellent radiochemical purity (100%), and acceptable molar activity (20–46 GBq μmol$^{-1}$). It is likely that molar activity would be increased by starting with higher initial activity. While macroscale studies were limited by the availability of precursor, this work establishes a connection between microscale and macroscale reactions and suggests the possibility of a rapid and economical approach for novel tracer development, *i.e.*, optimizing radiochemistry on a high-throughput microdroplet platform and then performing straightforward translation to vial-based systems to enable wider applicability to the existing install base of radiosynthesizer technology.

## Supplementary Material

Refer to Web version on PubMed Central for supplementary material.

## Acknowledgements

We thank Jeffrey Collins for producing [$^{18}$F]fluoride for these studies. Microfluidic reaction chips were produced in the UCLA Nanofabrication Laboratory (NanoLab), and we thank the staff for technical support. This work was funded in part by a Dissertation Year Fellowship (for YL) from UCLA Graduate Division, the National Institutes of Health (S10 OD026942), the National Institute of Biomedical Imaging and Bioengineering (T32 EB002101, R01 EB032264), and the National Cancer Institute (R33 CA240201). YH received financial support from China Scholarship Council (Project number: CSC201706040066).

## References

1. Shukla AK and Kumar U, J. Med. Phys, 2006, 31, 13–21. [PubMed: 21206635]
2. Papathanassiou D, Bruna-Muraille C, Liehn J-C, Nguyen TD and Curé H, Crit. Rev. Oncol. Hematol, 2009, 72, 239–254. [PubMed: 19091592]
3. Fowler JS and Wolf AP, Acc. Chem. Res, 1997, 30, 181–188.
4. Edem PE, Steen EJL, Kjær A and Herth MM, in Late-Stage Fluorination of Bioactive Molecules and Biologically-Relevant Substrates, ed. Postigo A, Elsevier, 2019, pp. 29–103.
5. Kuchar M and Mamat C, Molecules, 2015, 20, 16186–16220. [PubMed: 26404227]
6. Le Bars D, J. Fluorine Chem, 2006, 127, 1488–1493.
7. Cai L, Lu S and Pike VW, Eur. J. Org. Chem, 2008, 2008, 2853–2873.
8. Jacobson O, Kiesewetter DO and Chen X, Bioconjugate Chem, 2015, 26, 1–18.
9. Ajenjo J, Destro G, Cornelissen B and Gouverneur V, EJNMMI Radiopharm. Chem, 2021, 6, 33. [PubMed: 34564781]
10. Pike VW and Aigbirhio FI, J. Chem. Soc., Chem. Commun, 1995, 2215–2216.
11. World Intellectual Property Organization, WO2010117435A3, 2011.
12. Hull KL, Anani WQ and Sanford MS, J. Am. Chem. Soc, 2006, 128, 7134–7135. [PubMed: 16734446]
13. Watson DA, Su M, Teverovskiy G, Zhang Y, García-Fortanet J, Kinzel T and Buchwald SL, Science, 2009, 325, 1661–1664. [PubMed: 19679769]
14. Lee E, Kamlet AS, Powers DC, Neumann CN, Boursalian GB, Furuya T, Choi DC, Hooker JM and Ritter T, Science, 2011, 334, 639–642. [PubMed: 22053044]
15. Tredwell M, Preshlock SM, Taylor NJ, Gruber S, Huiban M, Passchier J, Mercier J, Génicot C and Gouverneur V, Angew. Chem., Int. Ed, 2014, 53, 7751–7755.
16. Mossine AV, Brooks AF, Makaravage KJ, Miller JM, Ichiishi N, Sanford MS and Scott PJH, Org. Lett, 2015, 17, 5780–5783. [PubMed: 26568457]
17. Chen W, Huang Z, Tay NES, Giglio B, Wang M, Wang H, Wu Z, Nicewicz DA and Li Z, Science, 2019, 364, 1170–1174. [PubMed: 31221856]
18. Makaravage KJ, Brooks AF, Mossine AV, Sanford MS and Scott PJH, Org. Lett, 2016, 18, 5440–5443. [PubMed: 27718581]
19. Taylor NJ, Emer E, Preshlock S, Schedler M, Tredwell M, Verhoog S, Mercier J, Genicot C and Gouverneur V, J. Am. Chem. Soc, 2017, 139, 8267–8276. [PubMed: 28548849]
20. Preshlock S, Calderwood S, Verhoog S, Tredwell M, Huiban M, Hienzsch A, Gruber S, Wilson TC, Taylor NJ, Cailly T, Schedler M, Collier TL, Passchier J, Smits R, Mollitor J, Hoepping A, Mueller M, Genicot C, Mercier J and Gouverneur V, Chem. Commun, 2016, 52, 8361–8364.
21. Mossine AV, Tanzey SS, Brooks AF, Makaravage KJ, Ichiishi N, Miller JM, Henderson BD, Skaddan MB, Sanford MS and Scott PJH, Org. Biomol. Chem, 2019, 17, 8701–8705. [PubMed: 31536095]
22. Zlatopolskiy BD, Zischler J, Krapf P, Zarrad F, Urusova EA, Kordys E, Endepols H and Neumaier B, Chem. – Eur. J, 2015, 21, 5972–5979. [PubMed: 25708748]

23. Hoffmann C, Kolks N, Smets D, Haseloer A, Gröner B, Urusova EA, Endepols H, Neumaier F, Ruschewitz U, Klein A, Neumaier B and Zlatopolskiy BD, Chem. – Eur. J, 2023, 29, e202202965. [PubMed: 36214204]
24. Mossine AV, Brooks AF, Bernard-Gauthier V, Bailey JJ, Ichiishi N, Schirrmacher R, Sanford MS and Scott PJH, J. Labelled Compd. Radiopharm, 2018, 61, 228–236.
25. Rensch C, Jackson A, Lindner S, Salvamoser R, Samper V, Riese S, Bartenstein P, Wängler C and Wängler B, Molecules, 2013, 18, 7930–7956. [PubMed: 23884128]
26. Kuge Y, Shiga T and Tamaki N, Perspectives on Nuclear Medicine for Molecular Diagnosis and Integrated Therapy, Springer, 2016.
27. Knapp K-A, Nickels ML and Manning HC, Mol. Imaging Biol, 2020, 22, 463–475. [PubMed: 31485889]
28. Wang J and van Dam RM, Mol. Imaging, 2020, 19, 1–21.
29. Elkawad H, Xu Y, Tian M, Jin C, Zhang H, Yu K and He Q, Chem. – Asian J, 2022, 17(20), e202200579. [PubMed: 35909081]
30. Pascali G, Watts P and Salvadori PA, Nucl. Med. Biol, 2013, 40, 776–787. [PubMed: 23684316]
31. Sergeev M, Lazari M, Morgia F, Collins J, Javed MR, Sergeeva O, Jones J, Phelps ME, Lee JT, Keng PY and van Dam RM, Commun. Chem, 2018, 1, 10. [PubMed: 34291178]
32. Iwata R, Pascali C, Terasaki K, Ishikawa Y, Furumoto S and Yanai K, J. Labelled Compd. Radiopharm, 2018, 61, 540–549.
33. Iwata R, Terasaki K, Ishikawa Y, Harada R, Furumoto S, Yanai K and Pascali C, Appl. Radiat. Isot, 2020, 109361. [PubMed: 32877862]
34. Lu Y, Wang J, van Dam RM and Hsiao A, Chem. Eng. J, 2022, 435, 134983.
35. Zhang X, Liu F, Knapp K-A, Nickels ML, Manning HC and Bellan LM, Lab Chip, 2018, 18, 1369–1377. [PubMed: 29658049]
36. Zhang X, Liu F, Payne AC, Nickels ML, Bellan LM and Manning HC, Mol. Imaging Biol, 2020, 22, 1370–1379. [PubMed: 32632739]
37. Keng PY, Chen S, Ding H, Sadeghi S, Shah GJ, Dooraghi A, Phelps ME, Satyamurthy N, Chatziioannou AF, Kim C-J and van Dam RM, Proc. Natl. Acad. Sci. U. S. A, 2012, 109, 690–695. [PubMed: 22210110]
38. Keng PY and van Dam RM, Mol. Imaging, 2015, 14, 7290.2015.00030.
39. Ghosh A, Ganguly R, Schutzius TM and Megaridis CM, Lab Chip, 2014, 14, 1538–1550. [PubMed: 24622962]
40. Wang J, Chao PH, Hanet S and van Dam RM, Lab Chip, 2017, 17, 4342–4355. [PubMed: 29164208]
41. Wang J, Chao PH and van Dam RM, Lab Chip, 2019, 19, 2415–2424. [PubMed: 31187109]
42. Lisova K, Chen BY, Wang J, Fong KM-M, Clark PM and van Dam RM, EJNMMI Radiopharm. Chem, 2020, 5, 1.
43. Wang J, Holloway T, Lisova K and van Dam RM, React. Chem. Eng, 2020, 5, 320–329. [PubMed: 34164154]
44. Sergeev M, Lazari M, Morgia F, Collins J, Javed MR, Sergeeva O, Jones J, Phelps ME, Lee JT, Keng PY and van Dam RM, Commun. Chem, 2018, 1, 10. [PubMed: 34291178]
45. Lu Y and van Dam RM, Nucl. Med. Biol, 2021, 96–97, S15–S16.
46. He Y, Schild M, Grether U, Benz J, Leibrock L, Heer D, Topp A, Collin L, Kuhn B, Wittwer M, Keller C, Gobbi LC, Schibli R and Mu L, J. Med. Chem, 2022, 65, 2191–2207. [PubMed: 35089028]
47. Rios A, Wang J, Chao PH and van Dam RM, RSC Adv, 2019, 9, 20370–20374. [PubMed: 35514735]
48. Wang J, Rios A, Lisova K, Slavik R, Chatziioannou AF and van Dam RM, Nucl. Med. Biol, 2020, 82–83, 41–48.
49. The Broad Scope of Cesium Salts in Organic Chemistry, Reference to a website: http://old.inno-chem.com.cn/pdf/4.pdf.
50. Jones J, Do V, Lu Y and van Dam RM, Chem. Eng. J, 2023, 468, 143524. [PubMed: 37576334]

51. Wang J, Chao PH, Slavik R and van Dam RM, RSC Adv, 2020, 10, 7828–7838. [PubMed: 35492189]

52. Lisova K, Wang J, Hajagos TJ, Lu Y, Hsiao A, Elizarov A and van Dam RM, Sci. Rep, 2021, 11, 20636. [PubMed: 34667246]

53. Zischler J, Kolks N, Modemann D, Neumaier B and Zlatopolskiy BD, Chem. – Eur. J, 2017, 23, 3251–3256. [PubMed: 27943464]

54. Tian J, He Y, Deuther-Conrad W, Fu H, Xie F, Zhang Y, Wang T, Zhang X, Zhang J, Brust P, Huang Y and Jia H, Bioorg. Med. Chem, 2020, 28, 115560. [PubMed: 32616183]

55. Jia H, Cai Z, Holden D, He Y, Lin S, Li S, Baum E, Shirali A, Kapinos M, Gao H, Ropchan J and Huang Y, ACS Chem. Neurosci, 2020, 11, 1673–1681. [PubMed: 32356969]

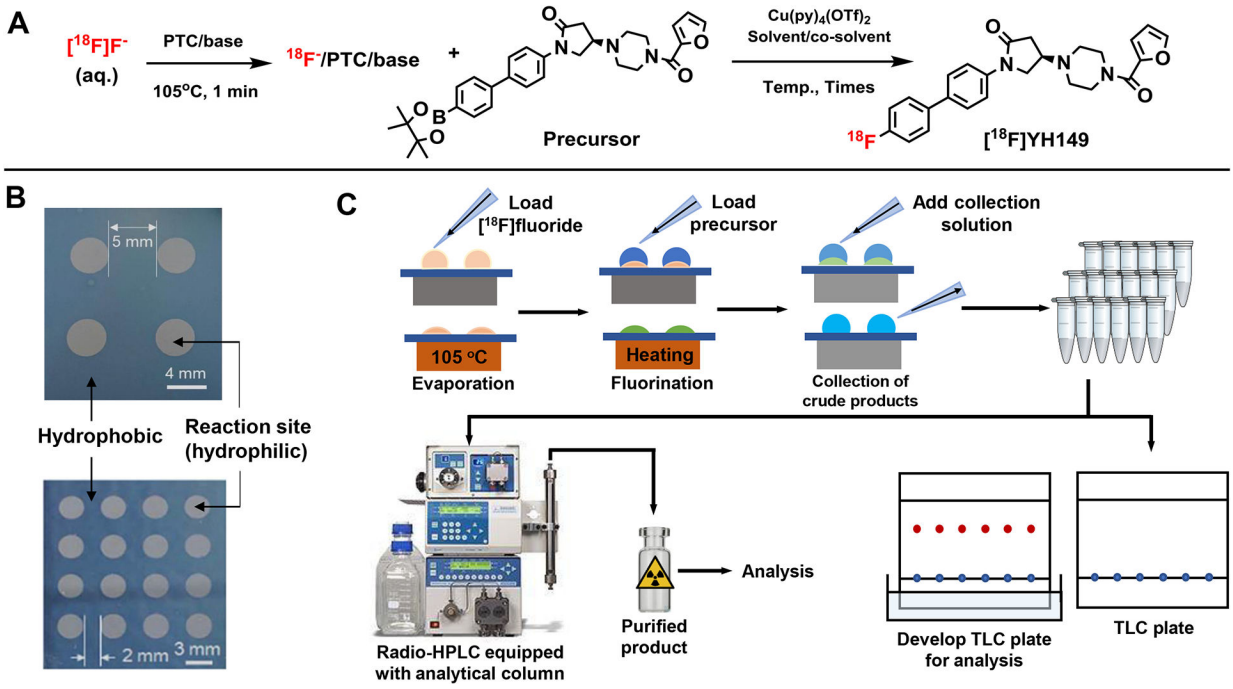


**Fig. 1.**

(A) [$^{18}$F]YH149 synthesis scheme. (B) 2×2 and 4×4 multi-reaction chips for high-throughput synthesis optimization. (C) Process flow for (parallel) droplet-based radiosynthesis. Subsequently, the collected crude products are subject to multi-lane radio-TLC analysis (for synthesis optimization) or radio-HPLC purification (for [$^{18}$F]YH149 production using a droplet system).

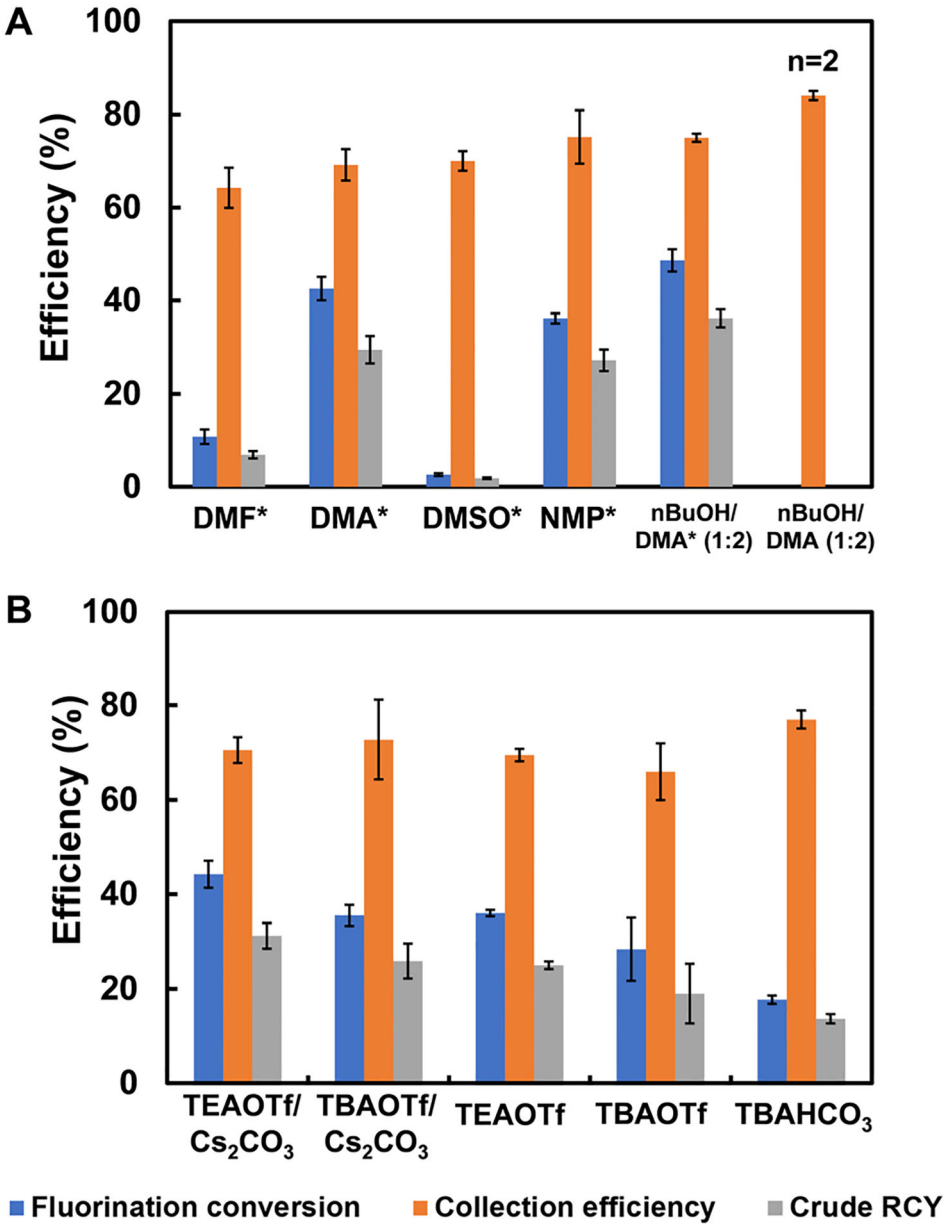


**Fig. 2.**

Influence of reaction parameters on the performance of the microdroplet radiosynthesis. (A) Impact of fluorination solvent / co-solvent. Solvent mixtures are all v/v, and asterisks "*" indicate that the solvent contains 4% pyridine. (B) Impact of type of phase transfer catalyst (PTC) and base used during [$^{18}$F]fluoride drying.

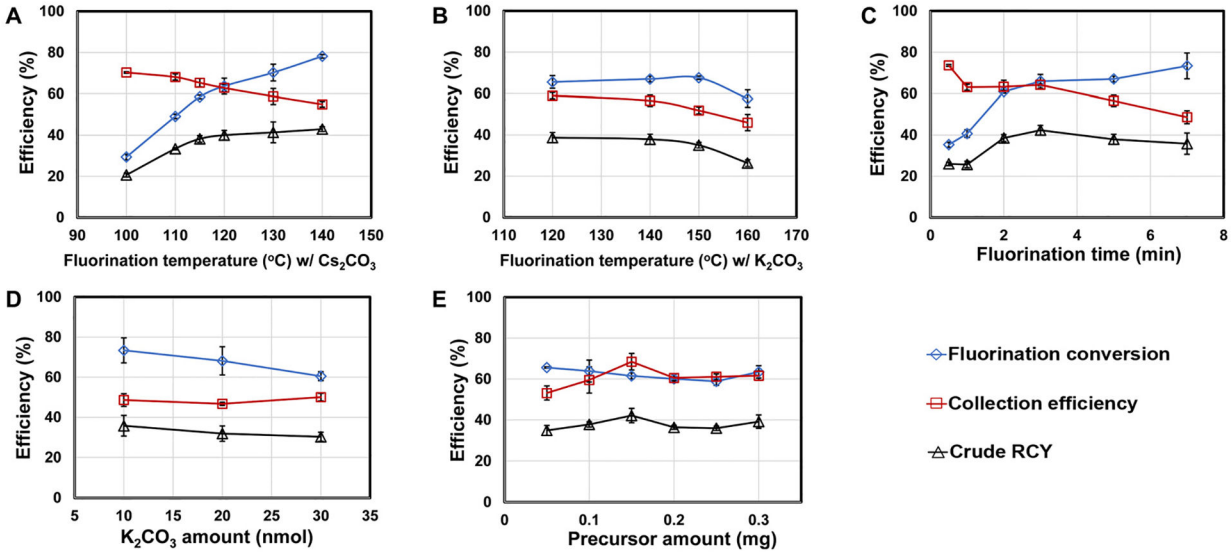


**Fig. 3.**

Influence of reaction parameters on the performance of the microdroplet radiosynthesis. (A, B) Impact of fluorination temperature for two base types. (C) Impact of reaction time. (D) Impact of amount of base. (E) Impact of amount of precursor.

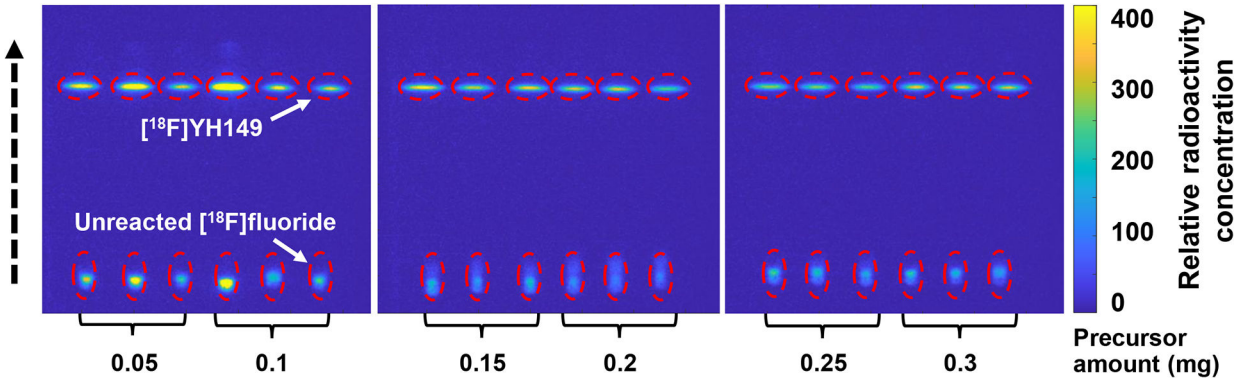


**Fig. 4.**

Example of high-throughput analysis of crude fluorination products (from study of precursor amount) using multi-lane TLC with Cerenkov luminescence imaging (CLI) readout.

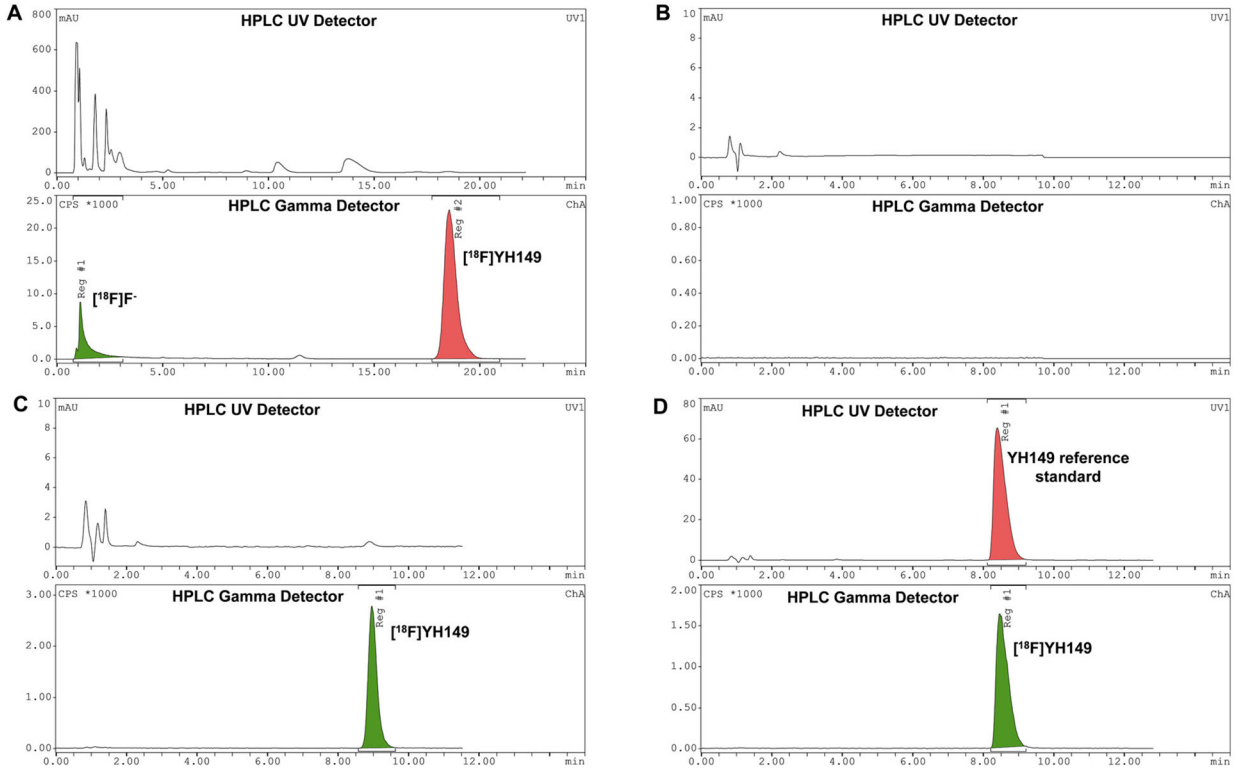


**Fig. 5.**

Example radio-HPLC chromatograms via droplet-based radiosynthesis: (A) crude [$^{18}$F]YH149, (B) blank injection of purification mobile phase, (C) purified [$^{18}$F]YH149, and (D) co-injection of [$^{18}$F]YH149 and YH149 reference standard. Note that retention times are different because panel A uses the purification mobile phase while other panels use a different analytical mobile phase.

**Table 1**

Summary of optimization experiments and findings. At each stage, the best performing condition was selected and held constant in later experiments.

| Day | Optimization study | Selected optimal condition |
|---|---|---|
| **1** | Initial attempts at droplet reaction | Use Condition B (in Table S1) |
| | Optimize solvent type | ←Solvent must contain pyridine<br>← DMA/nBuOH/pyridine (64:32:4, v/v) |
| **2** | Optimize PTC/base type | ← TEAOTf/$Cs_2CO_3$ |
| **3** | Optimize temperature and base type | ← 140°C<br>← TEAOTf/$K_2CO_3$ |
| **4** | Optimize reaction time | ← 3 min |
| | Optimize base amount | ← 10 nmol |
| **5** | Optimize precursor amount | ← 0.15 mg |
| | Additional solvent test | No change |
| | Additional base type test | ← TEAOTf/$Cs_2CO_3$ |

**Table 2**

Comparison of performance prior macroscale synthesis method, optimized droplet-based synthesis, and translated vial-based (macroscale) preparation.

| | mL-scale synthesis | Optimized droplet synthesis | Translated vial-based synthesis |
|---|---|---|---|
| | **He et al.** | **This work** | **This work** |
| Number of repeats (n) | 5 | 4 | 4 |
| Starting $^{18}F^-$activity (GBq) | 50–60 | 0.2–1.45 | 0.2–1.44 |
| Amount of PTC/base (μmol) | $K_2CO_3$ (0.7), $K_2C_2O_4$ (6), $K_{222}$ (16.7) | $Cs_2CO_3$ (0.01), TEAOTf (0.3) | $Cs_2CO_3$ (0.1), TEAOTf (3) |
| Amount of precursor (μmol) | 3.7–5.5 | 0.28 | 2.8 |
| Precursor concentration (mM) | 12.3–18.3 | 28 | 9.3 |
| Amount of $Cu(Py)_4(OTf)_2$ (μmol) | 20.6 | 0.68 | 6.8 |
| Reaction volume (μL) | 300 | 10 | 300 |
| Temperature (°C) | 110 | 140 | 140 |
| Reaction time (min) | 10 | 3 | 10 |
| Radiochemical yield (RCY, %)[a] | 4.4 ± 0.5 | 52 ± 8 | 50 ± 10 |
| Radiochemical purity (RCP, %)[b] | >99 | 100 | 100 |
| Product activity at EOS (GBq) | 1.8–3.02 | 0.080–0.623 | 0.058–0.410 |
| Molar activity (GBq/μmol) at EOS | 100–308 | 77–854 | 20–46 |
| Total preparation time (min) | 75 | 26[c] | 58[c] |

[a]RCY was obtained by radio-HPLC isolation and is calculated by dividing activity of collected pure product by initial activity and correcting for decay.

[b]RCP was determined by radio-HPLC.

[c]Product formulation was not included.

EOS = End of synthesis.